

Structure and dynamics of a molten globular enzyme

Konstantin Pervushin^{1,3}, Katherina Vamvaca^{2,4}, Beat Vögeli^{1,4} & Donald Hilvert²

Although protein dynamics has been recognized as a potentially important contributor to enzyme catalysis, structural disorder is generally considered to reduce catalytic efficiency. This widely held assumption has recently been challenged by the finding that an engineered chorismate mutase combines high catalytic activity with the properties of a molten globule, a loosely packed and highly dynamic conformational ensemble. Taking advantage of the ordering observed upon ligand binding, we have now used NMR spectroscopy to characterize this enzyme in complex with a transition-state analog. The complex adopts a helix-bundle structure, as designed, but retains unprecedented flexibility on the millisecond timescale across its entire length. Moreover, pre-steady-state kinetics data show that binding occurs by an induced-fit mechanism on the same timescale as the enzymatic reaction, linking global conformational plasticity with efficient catalysis.

Proteins are intrinsically flexible molecules that undergo conformational changes over a wide range of timescales and amplitudes. In enzyme catalysis, dynamic fluctuations can influence substrate binding and product release, and they may even shape the effective barrier for the catalyzed reaction^{1–4}. Nevertheless, how protein motions are coupled to catalysis remains poorly understood⁵.

Intrinsically disordered proteins, whose structures and dynamics alter dramatically as they perform their biological roles^{6,7}, represent potentially attractive systems for examining dynamical contributions to function. In previous experiments, we converted the intimately entwined homodimeric chorismate mutase from *Methanococcus jannaschii* (MjCM)⁸ into a functional monomer (mMjCM) by inserting the hinge-loop sequence ARWPWAEK into its long, dimer-spanning N-terminal helix (we refer to the loop positions as residues 23a–h)⁹. The topologically redesigned enzyme catalyzed the conversion of chorismate to prephenate, a key step in the biosynthesis of aromatic amino acids, with activity similar to that of the native enzyme ($k_{\text{cat}} = 3.2 \text{ s}^{-1}$, $K_{\text{m}} = 170 \text{ }\mu\text{M}$). Unexpectedly, however, it had biophysical properties associated with a non-native molten-globule state, including poor NMR signal dispersion, rapid hydrogen-deuterium exchange, noncooperative thermal denaturation and binding to 8-anilino-1-naphthalene sulfonate (ANS)¹⁰. Here we use spectroscopy and rapid kinetics measurements to characterize the structural changes that occur in this conformational ensemble upon binding of a transition-state analog (TSA)¹¹.

RESULTS

Solution structure of the mMjCM–TSA complex

Although extreme line broadening hinders structural characterization of the apoprotein, addition of ligand to mMjCM causes a transition from a disordered to a more ordered state¹⁰, opening the door to

detailed NMR spectroscopic studies. We determined the structure of the enzyme–TSA complex by standard three-dimensional NMR methods using NOEs and residual dipolar couplings¹². Aside from a few residues in or near the engineered loop (at positions 23, 23e–h and 24–28) and in the C-terminal helix (73, 77 and 80), which are broadened beyond detection, all backbone resonances and 89% of the protein side chains were assigned. The ensemble of the ten lowest-energy conformers has an r.m.s. deviation of 0.49 Å for all backbone atoms.

The protein folds as a four-helix bundle that closely matches the intended design⁹ (Fig. 1). Superposition of the helices in the mean mMjCM–TSA NMR structure (residues 5–22, 30–42, 49–66 and 70–97) with the corresponding segments in the crystal structure of the homologous chorismate mutase dimer from *Escherichia coli* (EcCM)¹³ yields an r.m.s. deviation of 0.9 Å. By comparison, the engineered loop is poorly restrained, and it probably adopts multiple conformations. Partial fraying of the adjacent N terminus of the second helix is also apparent. Nonetheless, the catalytic residues, which point toward the interior of the protein, form an active site that closely resembles that of EcCM and recognize the TSA in essentially the same way (Fig. 2).

At high protein concentrations, partial dimerization is evident. Consistent with analytical ultracentrifugation data affording a K_{a} value of 900 M^{–1} for self-association (Supplementary Fig. 1 online), the rotational correlation time of the complex increased from 5 ns to 10.6 ns when its concentration was raised from 70 μM to 0.6 mM (data not shown). Dimerization is mediated by a small number of intermolecular contacts near the engineered loop (Fig. 1d). In particular, interactions between the two exposed tryptophan residues from one polypeptide and the side chains of Leu24 and Ile72 from the other appear to be key. As expected from such an arrangement,

¹Laboratory of Physical Chemistry and ²Laboratory of Organic Chemistry, ETH Zurich, CH-8093 Zurich, Switzerland. ³Present address: School of Biological Sciences, Nanyang Technological University, 60, Nanyang Drive, Singapore 637551, Singapore. ⁴These authors contributed equally to this work. Correspondence should be addressed to K.P. (kpervushin@ntu.edu.sg) or D.H. (hilvert@org.chem.ethz.ch).

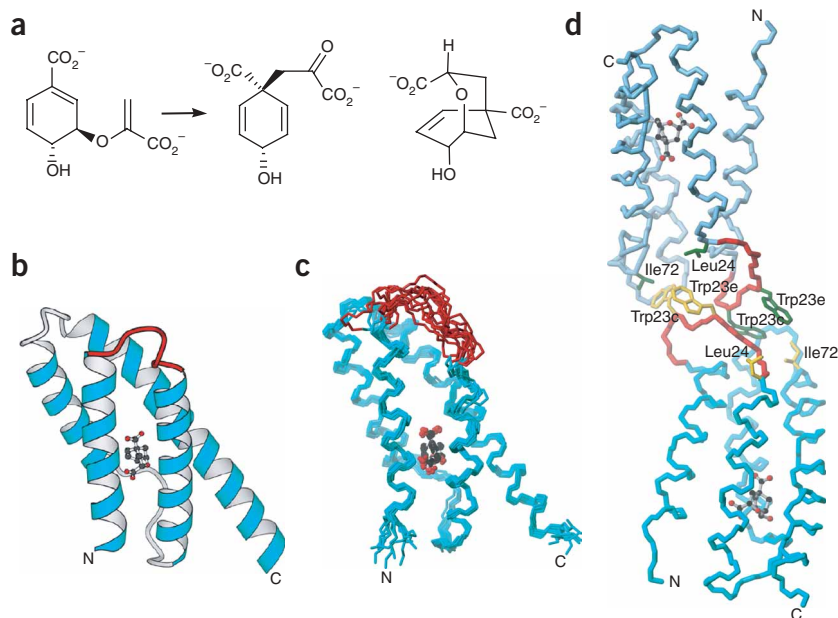


Figure 1 Structure of the topologically reengineered chorismate mutase mMjCM. (a) Left, conversion of chorismate to prephenate catalyzed by the enzyme. Right, a conformationally constrained oxabicyclic dicarboxylic acid TSA¹³. (b) Model of the 96-residue monomer based on the X-ray structure of the EcCM complex with the TSA. (c) The ten lowest-energy conformers of the mMjCM-TSA NMR structure. The engineered loop, residues 23a–h, is shown in red. The TSA, which binds at the active site, is shown in ball-and-stick representation. (d) Structure of the mMjCM dimer that forms at high protein concentration.

The R_{ex} rates are independent of protein concentration, eliminating dimerization as the cause of conformational exchange-induced line broadening (Supplementary Fig. 2 online). Ligand dissociation cannot account for these observations either, as shown by simulations of NMR spectra using experimental rate constants and observed chemical shift differences (see below and

replacement of Trp23c with lysine by mutagenesis strongly inhibits dimer formation without altering catalytic activity.

Protein dynamics

In addition to revealing the overall structure of the mMjCM complex, NMR spectroscopy enables analysis of protein motion on multiple timescales^{3,14,15}. We directly probed fast (picosecond to nanosecond) and slow (microsecond to millisecond) dynamic fluctuations in this system by measuring longitudinal and transverse relaxation of backbone ¹⁵N spins as well as heteronuclear ¹H-¹⁵N NOE relaxation. Generalized order parameters (S^2), internal correlation times (τ_c) and conformational exchange-induced line broadening (R_{ex}) were calculated from these data by the model-free approach^{16,17} (Supplementary Tables 1 and 2 online). The R_{ex} values were also measured independently using ¹⁵N chemical shift anisotropy/dipole-dipole cross-correlated relaxation at high and low protein concentrations (0.6 mM and 70 μ M, respectively; Supplementary Table 3 online).

S^2 order parameters, which reflect spatial restriction of ¹H-¹⁵N bonds on the picosecond-to-nanosecond timescale, range from 0 for unconstrained motion to 1 for completely rigid proteins. With the exception of the engineered loop, for which no data are available, the S^2 values for ligand-bound mMjCM are rather uniform, ranging between 0.66 and 0.95 (Fig. 3a). Their magnitude is characteristic of well-folded proteins, demonstrating that fast internal motions are limited in mMjCM^{3,17}. The τ_c values are also in the picosecond range, as is typical for a well-folded protein^{3,17}.

The dynamic behavior of the mMjCM-TSA complex is notably different on a slower timescale, as judged by pervasive conformational exchange-induced line broadening. The R_{ex} parameter monitors microsecond-to-millisecond fluctuations, with larger values corresponding to greater conformational diversity^{3,15,17}. For mMjCM, R_{ex} values are between 2 and 25 Hz, with an average of 12.7 Hz for all residues (Fig. 3a). Residues directly preceding the engineered loop are subject to greater conformational exchange-induced line broadening, and amide resonances of residues in the insert are broadened beyond detection ($R_{ex} > 30$ Hz; Fig. 3b).

Supplementary Fig. 3 online). The high relaxation rates thus seem to be an intrinsic feature of the mMjCM-TSA complex. Detailed characterization of conformational exchange would require Carr-Purcell-Meiboom-Gill (CPMG)-based relaxation dispersion measurements¹⁴, but poor sensitivity precluded quantitative analysis of mMjCM. On the basis of the likelihood that the frequency separation ($\Delta\omega$) of two extreme conformations in the exchanging ensemble is between 10 and 100 Hz, however, rate constants for conformational exchange in this protein can be estimated to range from 10 to 10^3 s⁻¹.

The millisecond conformational exchange processes throughout the mMjCM-TSA complex are unusual and imply a pervasive dynamic character that is atypical for conventional enzymes. In a well-folded protein, most residues have R_{ex} values below 5 Hz, and only a few positions—most often located in flexible surface loops, at subunit interfaces or in the active site—are subject to more extensive conformational exchange^{3,15,17}. A case in point is the TSA complex of *Bacillus subtilis* chorismate mutase, in which only 5 of 124 residues have R_{ex} values greater than 5 Hz (ref. 18). Our preliminary studies of the MjCM dimer suggest that it behaves like the *B. subtilis* enzyme in the presence and absence of ligand (data not shown). In contrast, it

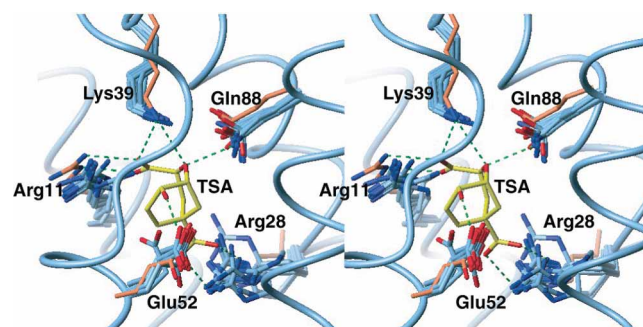


Figure 2 Stereo view of the mMjCM active site with bound TSA. The polar residues (cyan) that contact the TSA (yellow) are superimposed on their counterparts from the EcCM crystal structure (pink). Amino acid numbering is based on the EcCM sequence¹³.

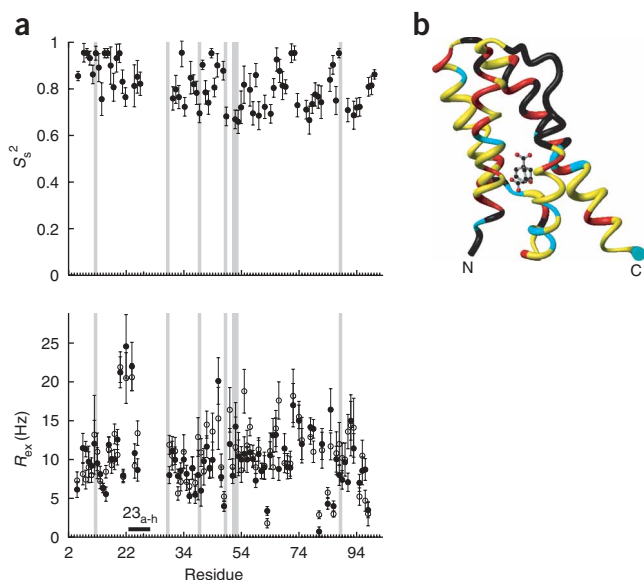


Figure 3 Enzyme dynamics on fast and slow timescales. **(a)** Order parameters S_s^2 (subscript *s* denotes ‘slow’) and conformational exchange-induced ^{15}N line-broadening rates R_{ex} at high (0.6 mM, filled circles) and low (70 μM , open circles) protein concentration. S_s^2 values were calculated using ModelFree and R_{ex} values were obtained from cross-correlation relaxation measurements. Gray lines mark positions of active site residues. **(b)** Spline representation of the enzyme with the tube radius set to $3 \times (1 - S_s^2)$, colored by R_{ex} of residues: cyan, $R_{\text{ex}} < 6.4 \text{ s}^{-1}$; yellow, $6.4 \text{ s}^{-1} < R_{\text{ex}} < 13 \text{ s}^{-1}$; red, $R_{\text{ex}} > 13 \text{ s}^{-1}$; black, unassigned R_{ex} values (prolines and residues whose backbone resonances are broadened beyond detection). The TSA bound in the active site is shown in ball-and-stick representation.

seems that the monomeric mMjCM–TSA complex lies somewhere between the molten-globule state, with its fluctuating tertiary structure, and a native state with an ordered structure that shows only small, localized motions.

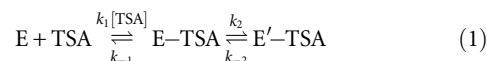
Pre-steady-state kinetics

We obtained evidence relating slow protein motions in mMjCM to molecular recognition processes at the active site by analyzing the pre-steady-state kinetics of ligand binding. The change in intrinsic protein fluorescence was monitored upon rapid mixing with various concentrations of prephenate (the product of the enzymatic reaction) or of the TSA. With prephenate, the data fit well to a single-exponential function, affording k_{on} and k_{off} values of $(1.4 \pm 0.3) \times 10^6 \text{ M}^{-1} \text{ s}^{-1}$ and $250 \pm 80 \text{ s}^{-1}$, respectively (Supplementary Fig. 4 online). The resulting equilibrium constant K_d (calculated as $k_{\text{off}}/k_{\text{on}}$) of $180 \mu\text{M}$ agrees well with the independently determined inhibition constant K_i of $190 \mu\text{M}$ for prephenate and is similar to the K_m value for chorismate ($170 \mu\text{M}$). $k_{\text{on}}[\text{L}]$ (where $[\text{L}]$ is ligand concentration) and k_{off} are both similar to the upper estimates of the rate constants for conformational exchange in mMjCM, suggesting that fluctuations in the protein conformational ensemble might gate substrate binding or product dissociation.

In contrast to the results with prephenate, the binding data for the TSA fit best to a double-exponential function (Fig. 4), from which two rate constants were extracted, one for a fast and one for a slow phase. The fast phase shows linear dependence on ligand concentration and represents the bimolecular binding process, yielding k_{on} and k_{off} constants of $(4 \pm 1) \times 10^4 \text{ M}^{-1} \text{ s}^{-1}$ and $8 \pm 2 \text{ s}^{-1}$, respectively. When plotted against TSA concentration, the rate constants for the slow phase increase hyperbolically (Fig. 4). The latter finding rules out

Figure 4 Pre-steady-state kinetics. Fluorescence intensity of mMjCM (2 μM) increases upon addition of the TSA (40 μM). Each trace was fit to a double-exponential decay function $F_t = F_1 e^{-k_{\text{fast}}t} + F_2 e^{-k_{\text{slow}}t} + F_3$, where F_t is the fluorescence at time t and k_{fast} and k_{slow} are the observed rate constants for the fast and slow phases, respectively. Similar measurements were performed at different ligand concentrations (40, 80, 160 and 320 μM), and the obtained rate constants for the fast phase (inset, top) and the slow phase (inset, bottom) were plotted against ligand concentration.

a binding mechanism that involves a shift in the pre-equilibrium population of the conformational ensemble, as such a model predicts an asymptotic decrease of the rate constants with increasing ligand concentration¹⁹. Instead, the data support an induced-fit mechanism^{19,20} (equation (1)), in which the molten-globule conformational ensemble (E) binds the TSA to give a ‘loose’ complex (E–TSA) that subsequently undergoes a relatively slow structural change to produce a ‘tight’ complex (E’–TSA):



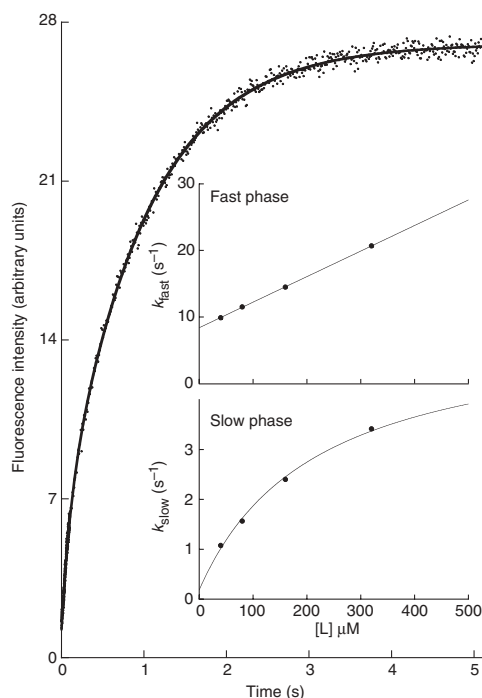
Fitting the data for the slow phase to the equation

$$k_{\text{slow}} = k_{-2} + k_2[\text{L}]/([\text{L}] + k_{-1}/k_1) \quad (2)$$

yields k_2 and k_{-2} values of 5.4 ± 0.2 and $0.2 \pm 0.1 \text{ s}^{-1}$, respectively. The overall dissociation constant calculated from these data (7 μM) is in good agreement with the equilibrium value determined by isothermal titration calorimetry (5 μM).

DISCUSSION

The induced-fit model is conventionally viewed as a conversion of one tight conformational ensemble (free enzyme) to another distinct ensemble (bound enzyme) through local substrate-mediated structural rearrangements. In contrast, free mMjCM exists as a



dynamic ensemble of α -helical conformers that rapidly interconvert on the millisecond timescale¹⁰. This molten state undergoes global conformational changes that ultimately lead to a structurally defined enzyme–ligand complex, albeit one that retains unusually high flexibility. Though probably stochastic in nature, internal motions in the complex may generate a collective dynamic matrix that samples catalytically active conformation(s) often enough to achieve rapid turnover in the presence of the true transition state. Although there is no evidence to suggest that fluctuations in the active site are directly coupled to the substrate such that they facilitate its conversion to product, the large reduction in enzyme dynamics in response to TSA binding implies widespread increases in noncovalent interactions throughout mMjCM. Such structural tightening has been suggested as a general means of increasing transition-state affinity and hence catalytic efficiency²¹. It is notable in this context that conversion of the initial-encounter complex to the high-affinity complex ($k_2 = 5.4 \text{ s}^{-1}$) occurs on the same timescale as enzyme turnover ($k_{\text{cat}} = 3.2 \text{ s}^{-1}$). This coincidence suggests that conformational changes may partially limit catalytic efficiency. Notably, though, the molten globular ensemble suffers no catalytic disadvantage relative to the parent MjCM dimer, a conventionally pre-folded scaffold, as both enzymes achieve identical 10^6 -fold rate accelerations ($k_{\text{cat}}/k_{\text{uncat}}$).

Once described as ‘kicking and screaming stochastic molecules’²², proteins span a continuum from totally disordered to well-folded structures. Enzymes have generally been placed at the upper end of this scale, their dynamic character being restricted to a small set of tightly folded conformations. Our findings expand this view, demonstrating that a highly dynamic, non-native conformational ensemble is compatible with efficient catalysis. Consequently, enzyme engineers might profit by shifting their focus from the design of structurally precise active sites to the creation of scaffolds with appropriate dynamic networks.

METHODS

Protein production and purification. The protein was produced and purified as described^{8,9}. For the production of ¹⁵N-labeled and ¹³C,¹⁵N-labeled proteins, Bioexpress growth medium (Cambridge Isotope Laboratories) containing additional nutrients was used (see **Supplementary Methods** online).

Nuclear magnetic resonance spectroscopy and data analysis. NMR experiments were performed at 20 °C on Bruker Avance 600-MHz and 900-MHz spectrometers, using (¹³C)¹⁵N-labeled protein samples in PBS buffer (20 mM sodium phosphate, 50 mM NaCl (pH 6.5)) supplemented with 5% D₂O. Backbone and side-chain resonances of mMjCM and TSA resonances were assigned by standard methods (see **Supplementary Methods**) and deposited in the Biological Magnetic Resonance Data Bank (see below). Assignments were verified by AutoLink and SideLink²³.

Restraints for backbone torsion angles were derived from C α and C β secondary chemical shifts. NOESY cross-peaks were assigned in the free enzyme model by CANDID²⁴ and DYANA²⁵. The obtained dihedral angles and NOE restraints, in combination with 50 ¹H-¹⁵N residual dipolar couplings measured in the presence of pfl phages and 40 protein–ligand NOE-derived restraints, were used to recalculate ten conformers of the mMjCM–TSA complex with XPLOR-NIH²⁶. To maintain a correct geometry¹³ for hydrogen bonds in the active site, 22 additional intermolecular restraints were imposed between the TSA and mMjCM donor and acceptor groups. These additional restraints altered neither the orientation of bound TSA nor that of catalytic residues. The resulting bundle of ten energy-refined DYANA conformers represents the solution structure of the mMjCM–TSA complex. The structure of the mMjCM dimer was calculated with CYANA²⁷ by explicit imposition of 18 additional NOE-derived restraints between two monomers. Statistical analysis showed that 87% of residues with assigned backbone resonances are in sterically favored regions of the Ramachandran map, with 10% and 3% in

Table 1 NMR and refinement statistics

mMjCM–TSA complex	
NMR distance and dihedral constraints	
Distance constraints	
Total NOE	1,410
Intra-residue	439
Inter-residue	931
Sequential ($ i - j = 1$)	325
Medium-range ($1 < i - j < 4$)	254
Long-range ($ i - j > 5$)	352
Intermolecular	40
Hydrogen bonds	97
Total dihedral angle restraints	
ϕ	62
ψ	62
Total ¹ H- ¹⁵ N residual dipolar couplings ^a	50
Structure statistics	
Violations (mean \pm s.d.)	
Distance constraints (Å)	1 \pm 1
Dihedral angle constraints (°)	2 \pm 1
Max. dihedral angle violation (°)	2.4 \pm 0.5
Max. distance constraint violation (Å)	0.5 \pm 0.1
Deviations from idealized geometry	
Bond lengths (Å)	0.03 \pm 0.01
Bond angles (°)	5 \pm 2
Impropers (°)	2 \pm 1
Average pairwise r.m.s. deviation ^b (Å)	
Heavy (residues 5–23 and 25–97) (Å)	1.33 \pm 0.21
Backbone (residues 5–23 and 25–97) (Å)	0.49 \pm 0.12

^aExperimental vs. calculated residual dipolar coupling correlation factor = 0.989 \pm 0.001. ^bPairwise r.m.s. deviation was calculated for ten refined structures.

additionally and generously allowed regions, respectively. No residues were found in the disallowed regions. NMR and refinement statistics are summarized in **Table 1**.

¹⁵N R₁, R₂ (refocused echo) and ¹H-¹⁵N heteronuclear NOE relaxation were measured at high (0.6 mM) protein concentration, whereas cross-correlated relaxation rates η_{xy} (ref. 28) were measured at both high (0.6 mM) and low (70 μ M) concentrations. In the ¹⁵N R_{1 ρ} relaxation dispersion experiments, the CPMG repetition rates varied from 70 to 1,000 Hz. The relaxation data were interpreted with ModelFree²⁹ and Fast ModelFree³⁰.

Stopped-flow measurements. TSA binding kinetics were followed with an Applied Photophysics SX.18MV stopped-flow instrument in PBS buffer at 20 °C. Samples were excited at 275 nm and fluorescence emission was monitored with a 305-nm-cutoff filter. Prephenate binding to mMjCM is too fast to be detected under these conditions and was monitored in 20%–50% (v/v) glycerol at 7.5 °C; rate constants were obtained by extrapolation to a glycerol concentration of 0 (**Supplementary Fig. 4**).

Accession codes. Protein Data Bank: Coordinates have been deposited with accession code 2GTV. BioMagResBank: accession code 7093.

Note: Supplementary information is available on the Nature Structural & Molecular Biology website.

ACKNOWLEDGMENTS

We are grateful to P. Anikeeva for carrying out preliminary NMR analysis, J. Beld for analytical ultracentrifugation studies, R. Kissner for technical assistance with stopped-flow experiments, and K. Woycechowsky for critical reading of the manuscript. This work was supported by the Schweizerischer Nationalfonds and the ETH Zurich. We dedicate this paper to the memory of D. Koshland.

AUTHOR CONTRIBUTIONS

K.P. and D.H. designed research; K.P. and B.V. did NMR experiments; K.V. did biochemical experiments; K.P., K.V., B.V. and D.H. analyzed data; K.P., K.V. and D.H. wrote the paper.

Published online at <http://www.nature.com/nsmb/>

Reprints and permissions information is available online at <http://npg.nature.com/reprintsandpermissions>

- Karplus, M. Dynamics of proteins. *Adv. Biophys.* **18**, 165–190 (1984).
- Hammes, G.G. Multiple conformational changes in enzyme catalysis. *Biochemistry* **41**, 8221–8228 (2002).
- Boehr, D.D., Dyson, H.J. & Wright, P.E. An NMR perspective on enzyme dynamics. *Chem. Rev.* **106**, 3055–3079 (2006).
- Hammes-Schiffer, S. & Benkovic, S.J. Relating protein motion to catalysis. *Annu. Rev. Biochem.* **75**, 519–541 (2006).
- Olsson, M.H.M., Parson, W.W. & Warshel, A. Dynamical contributions to catalysis: critical tests of a popular hypothesis. *Chem. Rev.* **106**, 1737–1756 (2006).
- Dyson, H.J. & Wright, P.E. Intrinsically unstructured proteins and their functions. *Nat. Rev. Mol. Cell Biol.* **6**, 197–208 (2005).
- Dunker, A.K., Brown, C.J., Lawson, J.D., Iakoucheva, L.M. & Obradovic, Z. Intrinsic disorder and protein function. *Biochemistry* **41**, 6573–6582 (2002).
- MacBeath, G., Kast, P. & Hilvert, D. A small, thermostable, and monofunctional chorismate mutase from the archeon *Methanococcus jannaschii*. *Biochemistry* **37**, 10062–10073 (1998).
- MacBeath, G., Kast, P. & Hilvert, D. Redesigning enzyme topology by directed evolution. *Science* **279**, 1958–1961 (1998).
- Vamvaca, K., Vögeli, B., Kast, P., Pervushin, K. & Hilvert, D. An enzymatic molten globule: efficient coupling of folding and catalysis. *Proc. Natl. Acad. Sci. USA* **101**, 12860–12864 (2004).
- Bartlett, P.A. & Johnson, C.R. An inhibitor of chorismate mutase resembling the transition-state conformation. *J. Am. Chem. Soc.* **107**, 7792–7793 (1985).
- Schwieters, C.D., Kuszewski, J.J., Tjandra, N. & Clore, G.M. The Xplor-NIH NMR molecular structure determination package. *J. Magn. Reson.* **160**, 65–73 (2003).
- Lee, A.Y., Karplus, P.A., Ganem, B. & Clardy, J. Atomic structure of the buried catalytic pocket of *Escherichia coli* chorismate mutase. *J. Am. Chem. Soc.* **117**, 3627–3628 (1995).
- Mittermaier, A. & Kay, L.E. New tools provide new insights in NMR studies of protein dynamics. *Science* **312**, 224–228 (2006).
- Palmer, A.G. & Massi, F. Characterization of the dynamics of biomacromolecules using rotating-frame spin relaxation NMR spectroscopy. *Chem. Rev.* **106**, 1700–1719 (2006).
- Lipari, G. & Szabo, A. Model-free approach to the interpretation of nuclear magnetic resonance relaxation in macromolecules. 1. Theory and range of validity. *J. Am. Chem. Soc.* **104**, 4546–4559 (1982).
- Jarymowycz, V.A. & Stone, M.J. Fast time scale dynamics of protein backbones: NMR relaxation methods, applications, and functional consequences. *Chem. Rev.* **106**, 1624–1671 (2006).
- Eletsky, A., Kienhöfer, A., Hilvert, D. & Pervushin, K. Investigation of ligand binding and protein dynamics in *Bacillus subtilis* chorismate mutase by transverse relaxation optimized spectroscopy-nuclear magnetic resonance. *Biochemistry* **44**, 6788–6799 (2005).
- Fersht, A. *Structure and Mechanism in Protein Science* (W. H. Freeman, New York, 1999).
- Koshland, D.E. & Neet, K.E. The catalytic and regulatory properties of enzymes. *Annu. Rev. Biochem.* **37**, 359–410 (1968).
- Williams, D.H., Stephens, E., O'Brien, D.P. & Zhou, M. Understanding noncovalent interactions: ligand binding energy and catalytic efficiency from ligand-induced reductions in motion within receptors and enzymes. *Angew. Chem. Int. Ed. Engl.* **43**, 6596–6616 (2004).
- Weber, G. Energetics of ligand binding to proteins. *Adv. Protein Chem.* **29**, 1–83 (1975).
- Masse, J.E. & Keller, R. AutoLink: automated sequential resonance assignment of biopolymers from NMR data by relative-hypothesis-prioritization-based simulated logic. *J. Magn. Reson.* **174**, 133–151 (2005).
- Herrmann, T., Güntert, P. & Wüthrich, K. Protein NMR structure determination with automated NOE assignment using the new software CANDID and the torsion angle dynamics algorithm DYANA. *J. Mol. Biol.* **319**, 209–227 (2002).
- Mumenthaler, C., Güntert, P., Braun, W. & Wüthrich, K. Automated combined assignment of NOESY spectra and three-dimensional protein structure determination. *J. Biomol. NMR* **10**, 351–362 (1997).
- Schwieters, C.D., Kuszewski, J.J. & Clore, G.M. Using Xplor-NIH for NMR molecular structure determination. *Prog. Nucl. Magn. Reson. Spectrosc.* **48**, 47–62 (2006).
- Güntert, P. Automated NMR protein structure calculation with CYANA. *Meth. Mol. Biol.* **278**, 353–378 (2004).
- Korzhnev, D.M., Billeter, M., Arseniev, A.S. & Orekhov, V.Y. NMR studies of Brownian tumbling and internal motions in proteins. *Prog. Nucl. Magn. Reson. Spectrosc.* **38**, 197–266 (2001).
- Mandel, A.M., Akke, M. & Palmer, A.G. Backbone dynamics of *Escherichia coli* ribonuclease HI: correlations with structure and function in an active enzyme. *J. Mol. Biol.* **246**, 144–163 (1995).
- Cole, R. & Loria, J.P. FAST-Modelfree: a program for rapid automated analysis of solution NMR spin-relaxation data. *J. Biomol. NMR* **26**, 203–213 (2003).